ELSEVIER

Journal of Power Sources 113 (2003) 81–100

JOURNAL OF POWER SOURCES

www.elsevier.com/locate/jpowsour

Abuse behavior of high-power, lithium-ion cells

R. Spotnitz[a,*], J. Franklin[b]

[a]*Battery Design Co., 2277 DeLucchi Dr., Pleasanton, CA 94588, USA*
[b]*Solvay Research and Technology, Rue de Ransbeek 310, B-1120 Bruxelles, Belgium*

Received 26 August 2002; accepted 10 September 2002

Abstract

Published accounts of abuse testing of lithium-ion cells and components are summarized, including modeling work. From this summary, a set of exothermic reactions is selected with corresponding estimates of heats of reaction. Using this set of reactions, along with estimated kinetic parameters and designs for high-rate batteries, models for the abuse behavior (oven, short-circuit, overcharge, nail, crush) are developed. Finally, the models are used to determine that fluorinated binder plays a relatively unimportant role in thermal runaway.

Keywords: Simulation; Thermal; Lithium-ion battery; Polyvinylidene fluoride; Binder

1. Introduction

With increasing interest in lithium-ion batteries for automotive applications, there is a need to better understand the abuse tolerance of these batteries. For example, that fluorinated binders, such as polyvinylidene fluoride (PVDF), react exothermically with lithium is of some interest because use of fluorinated binders is desirable. Fluorinated binders perform well and are easy to use. So, the question naturally arises, do fluorinated binders contribute to thermal runaway? Or, because fluorinated binders react in the negative electrode only above 200 °C, is the reaction a consequence of thermal runaway? If so, to what extent does it contribute to the overall heat release and thus aggravate thermal runway?

The question as to the role of fluorinated binders in thermal runaway can be addressed through mathematical modeling. Through modeling, the various reactions contributing to thermal runaway can be decoupled and so clarify what reactions cause thermal runaway. To achieve this end, the model should include the chemical reactions and the mechanisms for heat conduction and dissipation. Modeling is practically indispensable in resolving this issue, since it enables a broad range of compositions and conditions to be explored, without the need for assembling and testing an extensive number of large batteries.

Here, simulation results, based on a mathematical model for abuse tolerance (oven, short-circuit, overcharge, nail and crush), are presented. The simulations are based on the thermal behavior of lithium-ion battery materials. Before presenting the model, reviews of the abuse behavior of lithium-ion batteries and modeling work are presented.

2. Survey of abuse behavior of lithium-ion batteries

The following abuse tests are widely used to characterize the abuse tolerance of lithium-ion cells.

(a) Oven test: This test simply involves exposing the battery, at some initial temperature, to a higher temperature. For consumer batteries, an oven temperature of 150 °C is used (UL2054).
(b) Short-circuit: A low resistance (<5 mΩ) is connected across the terminals of the battery. The battery may be preheated. In this test, current flows through the battery generating heat. The battery is heated internally due to current flow, but the external circuit can dissipate heat also.
(c) Overcharge test: Current is forced through the cell up to some limiting voltage. Heat is generated by electrochemical reactions and by current flowing through the cell.
(d) Nail: A nail is forced through the battery at a prescribed rate (such as 8 cm/s). Heat is generated by current flowing through the cell, and by current flowing through the nail. Initially the nail is positioned outside of the battery wall and, when the test begins, is forced

* Corresponding author.
E-mail address: rspotnitz@batdesign.com (R. Spotnitz).

0378-7753/02/$ – see front matter
PII: S0378-7753(02)00488-3

Nomenclature

$a_{s,N}$	specific area of negative active (cm^2/g)
B_{MW}	molecular weight of binder (g/mol)
c_N^0	Li site concentration in negative (mol/cm^3)
c_O	moles of oxidizable solvent per unit volume of electrolyte (mol/cm^3)
c_R	moles of reducible solvent per unit volume of electrolyte (mol/cm^3)
c_S	moles of solvent per unit volume of electrolyte (mol/cm^3)
E_{neg}	voltage of negative versus lithium (V)
E_{pos}	voltage of positive versus lithium (V)
F	Faraday's constant (C/eq.)
H_{LiB}	enthalpy of lithium/binder reaction (J/mol)
H_{LiS}	enthalpy of lithium/solvent reaction (J/mol)
H_{NB}	enthalpy of negative/binder reaction (J/mol)
H_{NS}	enthalpy of negative/solvent reaction (J/mol)
H_P	enthalpy of positive decomposition reaction (J/mol)
H_S	heat of reaction for solvent decomposition (J/mol)
H_{SEI}	(J/mol)
i	current density per area of electrode (A/cm^2)
i_{Li}	current density corresponding to lithium metal deposition (A/cm^2)
i_{OC}	overcharge current density (A/cm^2)
I	inert material (mol)
k_d	rate constant for lithium deintercalation under short circuit conditions (mol/cm^2)
k_{Li}	scaling factor to relate moles of Li to area (cm^2/mol)
k_{LiB}	rate constant for Li/binder reaction (s^{-1})
k_{LiS}	rate constant for Li/solvent reaction (s^{-1})
$k_{m,N}$	mass-transfer coefficient for lithium diffusion in negative (cm/s)
k_{NB}	rate constant for negative/binder reaction (s^{-1})
k_{NS}	rate constant for SEI formation ($cm^3/(mol\ s)$)
k_P	positive decomposition rate constant (s^{-1})
k_S	solvent decomposition rate constant (s^{-1})
k_{SEI}	rate constant for SEI decomposition (s^{-1})
l_N	coating weight per area of negative (g/cm^2)
L_E	thickness of SEI layer (cm)
L_E^0	minimum thickness of SEI layer (cm)
L_i	thickness, i = N, P, or sep (cm)
L_N	thickness of the negative coating (cm)
L_P	thickness of positive coating (cm)
L_{pos}	thickness of positive (=L_P) (cm)
L_{sep}	thickness of separator
m_E	moles of SEI per unit area of negative (mol/cm^2)
m_{Li}	moles of Li metal per unit area of negative (mol/cm^2)
m_N	mass of the negative active material (g/cm^2)
m_{PO}	moles of positive active material in the oxidized state per unit area of positive (mol/cm^2)
m_{PR}	moles of positive active material in the reduced state (mol/cm^2)
$N_{crushed}$	number of cells "crushed" in crush test
$N_{shorted}$	number of cells shorted by nail in nail test
N_N	mol of Li per cm^2 of cell area ($mol/(cm^2\ s)$)
R_{LiB}	rate of lithium/binder reaction ($mol/(cm^2\ s)$)
R_{LiS}	rate of lithium/solvent reaction ($mol/(cm^2\ s)$)
R_{NB}	rate of negative/binder reaction ($mol/(cm^3\ s)$)
R_{NS}	rate of negative/solvent reaction ($mol/(cm^2\ s)$)
R_P	rate of positive decomposition ($mol/(cm^2\ s)$)
R_S	rate of solvent decomposition ($mol/(cm^3\ s)$)
R_{SEI}	rate of SEI decomposition ($mol/(cm^2\ s)$)
R_{sep}	separator resistance ($\Omega\ cm^2$)
S_N	heat source term for negative (W/cm^2)
S_P	heat source term for positive (W/cm^2)
S_S	heat source term for separator (W/cm^2)
w_B	weight fraction of binder in negative
w_N	weight fraction of negative active material in negative coating
x_b	fraction of carbon sites filled in bulk
x_s	fraction of carbon sites filled with Li at surface

Greek letters

ε_N	porosity of negative
ε_P	porosity of positive
v_N	volume fraction of negative active in negative coating
υ_{PS}	stoichiometry for solvent/oxygen reaction
υ_S	stoichiometry for electrochemical oxidation of solvent
υ_{LiS}	stoichiometry for lithium/solvent reaction
υ_{LiB}	stoichiometry for lithium/binder reaction
υ_{NB}	stoichiometry for negative/binder reaction
υ_{NS}	stoichiometry for negative/solvent reaction
ρ_E	molar density of SEI (mol/cm^3)
σ_i	conductivity of layer or material "i" ($\Omega^{-1}\ cm^{-1}$)

through the battery wall and into the battery at a constant speed. As the nail moves forward, forming direct shorts between adjacent electrode pairs, the current flowing through the nail itself decreases.

(e) Crush test: A bar is used to press down on the battery until a short-circuit initiates. Heat is generated throughout the battery due to discharge, and locally through the electrode pairs that are physically shorted.

The overcharge test can be the most severe as additional energy is added to the cell. The nail and crush tests can be enhanced by using overcharged batteries. The nail, crush, and short-circuit tests are somewhat similar, but have significant differences. In these three tests, heat is generated by rapid discharge of the battery. The short-circuit test allows the cell to discharge uniformly throughout the volume of the cell. The nail test allows the cell to discharge uniformly, but focuses heat (due to the nail) locally. In addition, the nail

test, since the nail penetrates the casing of the battery, allows volatile electrolyte to leave and react with air. The crush test allows the cell to discharge uniformly from the short, but heat is generated locally in the cell due to the short. If the battery is designed to form a good internal electrical contact when crushed, then the crush test will behave like a short-circuit test.

Only a few reports on the abuse behavior of large cells are available. Most of the published accounts of abuse behavior refer to small (<1.5 Ah) lithium-ion cells.

Fouchard et al. [14] reported the response of AA-size, lithium-ion cells to heating in an oven. They found the onset temperature for thermal runaway varied inversely with the degree of lithiation of the negative electrode (the greater the degree of lithiation the lower the onset temperature), while the thermal stability of the cell increased with increasing lithiation of the cathode. They reported that the composition of the electrolyte affected the thermal stability of the cell (ethylene carbonate/dimethyl carbonate (EC/DMC) was more stable than PC/DME), and that $LiMn_2O_4$ cathodes offered better thermal stability than $LiCoO_2$ or $LiNiO_2$ cathodes.

Kitoh and Nemoto [23] report the results of external short-circuit, overcharge, nail penetration, and oven tests with cylindrical, 100 Wh, $LiMn_2O_4$/carbon batteries. The batteries contained shutdown separators, fuses, and safety vents. In a 130 °C oven test, the battery can temperature seemed to stabilize near the oven temperature, but after about 80 min, the can temperature jumped to ∼190 °C. At this point, the battery vented, but did not ignite. About 40 min into the test, the battery exhibited a large increase in internal resistance, most likely due to melting of the separator. In a short-circuit test, an external load of 6.0 mΩ was used compared to a battery impedance of ∼5 mΩ. Once shorted, the battery discharged at ∼15*C* rate for ∼80 s; this corresponds to ∼33% of the total capacity. At ∼80 s, the cell vented and the battery continued to discharge at a decreasing rate. Most likely, the decrease in current was partly due to shutdown of the separator. If the short-circuit test was carried out with an external load of 0.2 mΩ, the current was immediately cut-off due to a fuse inside the battery. In an overcharge test, a 1*C* current was applied with a voltage limit of 10 V. When the can temperature reached ∼100 °C, the current dropped dramatically due to shutdown of separator, and the test was discontinued. In a nail penetration test (nail speed 1 mm/s), the cell vented immediately after the nail was inserted. The battery reached a maximum temperature of 380 °C, but did not ignite.

Leising et al. [26] examined the overcharge and short-circuit behavior of 1.5 Ah prismatic lithium-ion cells. With a thermocouple placed inside the cell, they measured the internal temperature versus time and found it increased to a maximum of ∼132 °C (melting point of polyethylene separator) whereas the outside surface of the case reached a maximum temperature of 94 °C. In overcharge tests, they confirmed the finding of Tobishima and Yamaki [24] that low charging rates (<*C*/5) did not result in thermal runaway, while higher rates (*C*) did. By constructing cells with varying ratios of cathode to anode, they found the amount of charge leading to thermal runaway depended only on the amount of cathode material; runaway occurs near complete delithiation of the cobalt oxide. They found that cell rupture occurred when the internal cell temperature exceeded ∼190 °C and suggest that rupture is due to melting of metallic lithium formed at the negative electrode. However, if the cell is designed so lithium metal cannot deposit, it will still rupture, but at a higher temperature.

In overcharge studies of 18,650-size cells by five different manufacturers, Saito et al. [25] found that the heat released on overcharge was almost proportional to the charging current. They found that with a 0.2*C* charging rate, at around 160–180% overcharge, the heat generated in cells with $LiCoO_2$ cathodes increased dramatically; a cell with an $LiMn_2O_4$ cathode exhibited a big increase in heat generation at about 110% overcharge. With further overcharging, the heat generated in the cell became equal to the electrical energy input. Using a square wave to overcharge the cell, they showed that shutting off the current flow to the cell stopped heat generation. They suggest that thermal runaway is the result of solvent oxidation products, formed above 4.6 V, that react with the positive electrode material.

Maleki et al. [27] looked at the overcharge behavior of different lithium-ion cells with the objective of elucidating the roles of the positive and negative electrodes. Accelerating rate calorimetry (ARC) studies of the full cells (type A) and their individual electrodes indicate the positive electrode is responsible for thermal runaway at 50 and 100% state of charge (SOC), while the negative electrode is responsible for thermal runaway at 150 and 200% SOC. Above 100% SOC, the onset temperature of chemical reactions for the negative electrode decreased from >180 to ∼80 °C. This suggests that metallic lithium plays an important role in thermal runaway during overcharge.

Biensan et al. [4] report nail tests done on 4/5 A-size cells with different negative electrode binders and positive electrode materials. They found the safe voltage was higher with cobalt oxide cathodes than with nickel oxide cathodes, and with non-fluorinated binder than with polyvinylidene fluoride binder.

Dahn [34], using a nail with an embedded thermocouple, found that, with 18,650-size $LiCoO_2$ cells, the nail temperature exceeds 600 °C when forced slowly into the cell to a depth <4.5 mm. However, with a fast, deep nail penetration (7.5 mm), the nail temperature did not exceed 140 °C.

Tobishima and Yamaki [24] explain that the abuse tolerance of lithium-ion cells depends on the relative rates of heat removal and heat generation. When a cell cannot transfer heat to its environment at a rate equal to or higher than the rate of heat generation, it will undergo thermal runaway. They also present results from various abuse tests of small lithium-ion cells. In the overcharge test of prismatic cells (Al case, 600 mAh), cells did not vent at 1 or 1.5*C* rate of

overcharge, but caught fire at a 2*C* rate overcharge. In oven tests of cylindrical cells (1270 mAh), the cells were stable at 150 °C but smoked at 155 °C. Nail penetration tests with prismatic cells (835 mAh) did not overheat; however, cells that were slightly overcharged (0.03 V higher than standard voltage) did overheat and give off smoke. Similarly, a crush test of a cylindrical cell (720 mAh) charged according to the manufacturer's recommendation did not smoke, but an overcharged cell did catch fire. The fire is attributed by the authors to lithium metal formation.

While there is little information published about abuse testing of lithium-ion cells, there is virtually no material available on abuse testing of modules. The concern is that thermal runaway of a single cell will induce runaway of an entire module. Modules envisioned for hybrid electric vehicles (HEVs) consist of at least 10 cells, so runaway of a module is potentially at least an order of magnitude more energetic than thermal runaway of a single cell.

3. Survey of thermal behavior of components in lithium-ion batteries

Abuse testing of batteries gives some insight into failure mechanisms, but direct characterization of the materials that constitute the battery can lead to an understanding of what makes a battery abuse tolerant. Below, the important exothermic reactions that take place during abuse testing of lithium-ion batteries are summarized, and then the literature supporting each reaction reviewed in order to extract quantitative information useful for modeling.

The following exothermic reactions have been proposed to take place during abuse testing of lithium-ion batteries.

(a) Solid electrolyte interface (SEI) layer decomposition: The negative electrode is protected from direct reaction with solvent by an electronically insulating but ionically conducting film called the ''solid electrolyte interface''. This layer is metastable and can decompose exothermically at 90–120 °C.
(b) Reaction of intercalated lithium with electrolyte: At elevated temperatures (>120 °C), the SEI layer does not protect the negative electrode from contact with the electrolyte and an exothermic reaction between intercalated lithium and electrolyte can occur.
(c) Reaction of intercalated lithium with fluorinated binder: Fluorinated binder can react exothermically with lithiated carbon.
(d) Electrolyte decomposition: The electrolyte can decompose exothermically at elevated temperatures (>200 °C).
(e) Positive active material decomposition: In the oxidized state, the positive active material can decompose exothermically and give off oxygen. This oxygen can react exothermically with electrolyte. Or, perhaps the positive material reacts directly with electrolyte. In any case, the chemical reduction of the positive active material is highly exothermic.
(f) On overcharge, metallic lithium is formed which can react with electrolyte.
(g) Lithium metal can react with binder.
(h) Discharge of the battery releases heat due to entropy changes, overpotentials, and ohmic resistances.

The literature supporting each of these exothermic processes is reviewed below.

3.1. SEI layer decomposition

Richard and Dahn [7] identifies an exothermic peak due to SEI decomposition in ARC studies of carbon anodes in electrolyte at ~100 °C. The peak is relatively insensitive to the amount of lithium intercalated into the carbon and does not appear if fresh carbon is heated with electrolyte. The SEI layer is assumed to consist of stable (such as Li_2CO_3), and metastable components (such as $(CH_2OCO_2Li)_2$). The metastable component might exothermically react as follows:

$$(CH_2OCO_2Li)_2 \rightarrow Li_2CO_3 + C_2H_4 + CO_2 + \tfrac{1}{2}O_2 \quad (1a)$$

or

$$2Li + (CH_2OCO_2Li)_2 \rightarrow 2Li_2CO_3 + C_2H_4 \quad (1b)$$

This depletion of the metastable SEI component gives rise to a peak in the ARC experiment. The composition of the SEI depends on the electrolyte composition. $LiBF_4$-based electrolytes do not exhibit a peak in the self-heating rate profile. With $LiPF_6$-based electrolytes, the shape and behavior of the peak depend on the solvents used. For example, EC:diethyl carbonate (DEC) (1:1) gives a shoulder on the main peak, whereas EC:DEC (1:2) does not.

From ARC measurements made at various initial temperatures (plots of $\ln dT/dt$ versus $1/T$) an activation energy of 1.35 kJ/mol and a frequency factor of 1.7×10^{15} s^{-1} were obtained. The ARC peak attributed to SEI decomposition (1 M $LiPF_6$ in EC:DEC (1:2), MCMB carbon) raises the sample temperature about 15 °C, which corresponds to 257 J/g of carbon. Increasing the surface area increased the amount of SEI and correspondingly the magnitude of the associated enthalpy.

Dahn's group has examined a number of carbon electrode materials (fibers, MCMB, coke, and synthetic graphites) using ARC [29] and found the initial temperature rise is proportional to the surface area of the carbon, with the exception of graphite.

Maleki et al. [3] in differential scanning calorimetry (DSC) studies of lithiated carbons with electrolyte observed a peak at ~100 °C that they attributed to thermal decomposition of the SEI layer.

Zhang et al. [2] reported DSC results for mixtures of lithiated carbon (MCMB-28) and electrolyte (1 M $LiPF_6$ in

1:1 EC:DMC). They found a peak beginning at ~130 °C that was small and independent of the degree of lithium intercalation; the peak was typically ~40 J/g, though a maximum value of 120 J/g was observed. If the sample was 70 wt.% active material and 8 wt.% binder, then the worst case heat of reaction is 186 J/g of carbon.

3.2. Reaction of intercalated carbon with electrolyte

Solvent might react with lithium (either metallic or intercalated) as follows:

$$2Li + C_3H_4O_3\ (EC) \rightarrow Li_2CO_3 + C_2H_4 \quad (2a)$$

$$2Li + C_4H_6O_3\ (PC) \rightarrow Li_2CO_3 + C_3H_6 \quad (2b)$$

$$2Li + C_3H_6O_3\ (DMC) \rightarrow Li_2CO_3 + C_2H_6 \quad (2c)$$

Roth et al. [28] reported DSC studies of lithiated carbon anodes (from Sony 18,650 cells) and EC:PC:DEC/$LiPF_6$ electrolytes. The lithiated carbon anode, when dried, showed peaks above 300 °C. Interestingly, addition of solvent without salt had no effect on the traces. However, in the presence of electrolyte (solvents + salt), the traces became very complex with peaks at ~100, ~150, ~270, and ~300 °C.

Richard and Dahn [7] studied the thermal stability of lithium intercalated graphite in electrolyte by differential scanning calorimetry and ARC. For the reaction of lithiated carbon (MCMB) and electrolyte (1 M $LiPF_6$ in 1:2 EC:DEC), they report an enthalpy of 1714 J/g of carbon. Since $Li_{0.8}C_6$ was used, the reaction enthalpy for intercalated lithium can be adjusted to 1.54×10^5 J/mol of lithium. They report activation energy of $E_a = 1.35 \times 10^5$ J/mol, and a frequency factor of $2.5 \times 10^{13}\ s^{-1}$.

Biensan et al. [4] report thermal studies of components from lithium-ion cells. For $LiPF_6$ in 1:1:3 PC:EC:DMC electrolyte, they found a peak at ~120 °C (350 J/g) attributed to Li_xC_6 + electrolyte. The paper does not specify if the heat of reaction is normalized with respect to the carbon or electrode material, or electrode material and electrolyte. Assuming the enthalpy refers to grams of carbon, and taking the capacity of the carbon as 330 mAh/g gives 2.84×10^4 J/mol of lithium. The use of $LiBF_4$ and LiTFSI salts resulted in dramatically different DSC traces. However, the enthalpies for the reaction with lithiated carbon were not reported.

Lampe-Onnerud et al. [11] report a heat of reaction of 1497 J/g for the reaction of LiC_6 + EC/DMC-$LiPF_6$ with an activation energy of 34 kJ/mol. Assuming a capacity of 330 mAh/g, this gives a reaction enthalpy of 1.2×10^5 J/mol of lithium.

Du Pasquier et al. [18] reported the enthalpies for the sum of SEI decomposition and lithiated carbon (MCMB 25–28)/electrolyte (1 M $LiPF_6$ in 2:1 EC:DMC) reactions. The enthalpy depended on the degree of lithiation; assuming a capacity of 330 mAh/g for MCMB and averaging their values gives $7.5 \pm 1.3 \times 10^4$ J/mol of lithium.

3.3. Reaction of lithiated carbon with fluorinated binder

Du Pasquier et al. [18] suggested that lithium (either metallic or intercalated) can react with a fluorinated binder as follows:

$$-CH_2-CF_2- + Li \rightarrow LiF + -CH{=}CF- + \tfrac{1}{2}H_2 \quad (3)$$

Alternatively, fluorinated binder might react according to this scheme:

$$2Li + RF_2 \rightarrow 2LiF + \tfrac{1}{2}R_2 \quad (4)$$

where the molecular weight of RF_2 is 64 g/(g mol).

Typically, a negative electrode contains about 8–12 wt.% binder with the balance being carbon. If the electrode is 8 wt.% binder, the carbon has a capacity of 330 mAh/g, then a fully charged electrode contains

$$\begin{aligned}&(330\,\text{mAh/g C}_6)(0.92\,\text{g C}_6\text{/g electrode})\\&\quad\times(3.6\,\text{A s/mAh})(1/96,500)(\text{mol Li/A s})\\&=0.0113\,\text{mol Li/g electrode}\end{aligned}$$

$$\begin{aligned}&(0.08\,\text{g PVDF/g electrode})(2\,\text{mol F/mol PVDF})\\&\quad\times(1/64)(\text{mol PVDF/g PVDF})\\&=0.0025\,\text{mol F/g electrode}\end{aligned}$$

So a fully-charged negative contains at least four times as many moles of Li than moles of fluorine. At first sight, this excess of lithium seems inconsistent with lithium fluoride formation as the reaction product, since DSC studies [10] with 8 wt.% PVDF binder indicate the heat of Li_xC_6/binder reaction increases linearly with degree of lithiation of the negative. On the other hand, other workers [4] report that the heat of reaction increases linearly with the amount of PVDF binder from 10 to 15% binder. This discrepancy might be due to the availability of lithium during the DSC experiment. Since lithium must diffuse through graphite to reach the PVDF binder, not all the lithium is available for reaction (indeed, the Li and the PVDF are not in the same place, initially at least, so the mere stoichiometric ratio is not very meaningful). As the degree of lithiation increases, more lithium becomes available for reaction. On the other hand, when the carbon is fully lithiated, the reaction with PVDF is limited by PVDF.

Du Pasquier et al. [18] reported the enthalpies for the reaction of lithiated carbon and lithium with various fluorinated binders. The authors suggest that LiC_6 reacts at lower temperatures than lithium metal due to the higher surface area of the carbons. They found, through X-ray analysis of the reaction products, that LiF is the major inorganic product. For PVDF homopolymer, assuming a Li_xC_6 capacity of 330 mAh/g gives 1.49×10^5 J/mol of LiC_6.

Maleki et al. [3] report a value of 317 J/g for the reaction of Li_xC_6 with PVDF; the reaction begins at ~200 °C and reaches a maximum at 287 °C. Later, Maleki et al. [10] reported a more in-depth study of the lithiated carbon/binder

reaction in which various carbons and various binders were examined. The authors explain that hard carbon (HC-1227) produces an exothermic DSC peak even when uncharged due to reaction of "irreversible lithium" with PVDF. The irreversible lithium is produced during SEI formation on the first charging cycle. It is interesting to note that the SFG-44 produces more heat than the MCMB even at the same state of charge. Since SFG-44 has a higher surface area than MCMB, this is consistent with the proposal that the reaction is diffusion-controlled. In any case, using the slopes from plots of heat of reaction versus charge, gives 7.2×10^4 J/mol Li (SFG-44), 5.9×10^4 J/mol Li (MCMB), and 3.8×10^4 J/mol Li (HC-1227).

Biensan et al. [4] report a value of 1500 J/g for the reaction of Li_xC_6 with PVDF; the reaction begins at ~240 °C, peaks at ~290 °C, and is complete at ~350 °C.

3.4. Electrolyte decomposition

Published work on electrolyte decomposition is somewhat contradictory and, in any case, the situation is complicated by interactions of the electrolyte and the cathode. For example, ethylene carbonate decomposes to carbon dioxide and ethylene oxide; ethylene oxide can exothermically decompose. The decomposition of EC is catalyzed by lithium nickelate [13]. Other workers have found that the amount of heat released in the reaction between $Li_{0.5}CoO_2$ and electrolyte is not affected by amount of electrolyte, within certain limits, but the amount of heat released in the reaction between $Li_xMn_2O_4$ and electrolyte increases with increasing electrolyte [16].

Sloop et al. [30] studied the stability of $LiPF_6$-EC:DMC electrolytes at 85 °C. Their results indicate that PF_5 gas, in equilibrium with $LiPF_6$ ($LiPF_6 \rightarrow LiF + PF_5$) reacts preferentially with EC over DMC to form soluble oligomers of ethylene carbonate as well as insoluble precipitates (perhaps phosphate esters).

Botte et al. [9] studied the thermal stability of $LiPF_6$-EC:EMC electrolytes. They found the thermal behavior was very sensitive to the electrolyte composition. For EC:EMC mixtures they report DSC traces that exhibit a slight endotherm before a broad exotherm. For 1 M $LiPF_6$ solutions, they report an enthalpy of ~300 J/g of electrolyte. The solvent concentration is taken as 0.0087 mol/g, which gives 3.43×10^4 J/mol of solvent.

Biensan et al. [4] report a heat of reaction of 250 J/g for decomposition of $LiPF_6$-PC:EC:3DMC electrolyte.

Kawamura et al. [43] report DSC studies of various solvents. They found that diethyl carbonate was more reactive than dimethyl carbonate in either propylene carbonate or ethylene carbonate and $LiPF_6$ or $LiClO_4$. For 1 M $LiPF_6$ electrolytes, they found exotherms between 230 and 280 °C with heats of reaction ~375 J/g (1:1 PC:DMC or EC:DMC) and 515 J/g (1:1 PC:DEC or EC:DEC). Addition of 1 wt.% water to the electrolytes reduced the magnitude of the exotherms by about a factor of two.

3.5. Positive active material decomposition

Charged positive active materials can disproportionate at elevated temperatures as follows [33]:

$$Ni_{0.8}Co_{0.2}O_2 \rightarrow \tfrac{1}{3}Ni_{2.4}Co_{0.6}O_4 + \tfrac{1}{3}O_2 \quad (5a)$$

$$Mn_2O_4 \rightarrow Mn_2O_3 + \tfrac{1}{2}O_2 \quad (5b)$$

The oxygen released might react with solvent as follows:

$$\tfrac{5}{2}O_2 + C_3H_4O_3\,(EC) \rightarrow 3CO_2 + 2H_2O \quad (6a)$$

$$4O_2 + C_4H_6O_3\,(PC) \rightarrow 4CO_2 + 3H_2O \quad (6b)$$

$$3O_2 + C_3H_6O_3\,(DMC) \rightarrow 3CO_2 + 3H_2O \quad (6c)$$

The work of Arai et al. [44] suggests, for delithiated lithium nickelate, that oxygen released by decomposition of Li_xNiO_2 completely combusts solvent according to reaction (6).

MacNeil and Dahn [8] studied the reaction kinetics for Li_xCoO_2 in non-aqueous electrolyte. They report a good fit with their data using a reaction enthalpy of 265 J/g of $LiCoO_2$; multiplying by the molecular weight of $LiCoO_2$ and assuming 0.5 eq. of Co^{4+}/mol of $Li_{0.5}CoO_2$ gives 5.18×10^4 J/eq. They report an activation energy of 1.235×10^5 J/eq., and a frequency factor of 6.67×10^{11} s^{-1}.

Biensan et al. [4] report enthalpies for several different electrolyte/positive electrode reactions; for $Li_{0.45}CoO_2$, 450 J/g are released between 220 and 500 °C.

Lampe-Onnerud et al. [11] report the heat of reaction for $Li_{0.5}CoO_2$ + EC/DMC-$LiPF_6$ occurs with two DSC peaks (total 615 J/g). The first exothermic process has an activation energy of 70 kJ/mol.

Venkatachalapathy et al. [1] reported ARC/DSC studies in which they found ΔH of 641.7 J/g for $Li_xNi_{0.8}Co_{0.2}O_2$ and 381 J/g for Li_xCoO_2. Unfortunately, the stoichiometry (x) of the materials was not disclosed. These authors also reported the thermal behavior of $LiNi_{0.8}Co_{0.2}O_2$ in 18,650-size lithium-ion cells [6]. DSC studies of the individual fully-charged electrodes taken from the cells show two exotherms (one minor and one large) for the negative and one major exotherm for the positive electrode. The ΔH for the carbon electrode is 317 and 641 J/g for the $LiNi_{0.8}Co_{0.2}O_2$ electrode. Assuming the carbon electrode is 90% active material and using 72 g/(g mol) for carbon gives 3.17×10^4 J/eq. for the LiC_6/solvent reaction. Similarly, assuming the $LiNi_{0.8}Co_{0.2}O_2$ electrode contains 85% active material and 196 g/eq. gives 1.48×10^5 J/eq. for the $LiNi_{0.8}Co_{0.2}O_2$/solvent reaction.

Maleki et al. [3] reported the DSC behavior of positive electrodes containing Sn-doped $LiCoO_2$. Washed samples showed an exotherm (146 J/g) stretching from 178 to 250 °C. Unwashed samples showed an exotherm (407 J/g) beginning at 167 °C and reaching a peak at 214 °C.

Lu et al. [6] reported the thermal behavior of delithiated $Li_{1-x}NiO_2$. They found the ΔH for thermal decomposition increased linearly with increasing x from $x = 0$–0.5 to a maximum of ~115 J/g; beyond $x = 0.5$ the enthalpy actually

decreased slightly with increasing x. For $x = 0.5$, the enthalpy corresponds to 2.25×10^4 J/eq. of NiO_2.

Zhang et al. [2] carried out DSC studies of positive electrode materials with electrolyte (1 M $LiPF_6$ in 1:2 EC:DMC). They found the heat generated increased almost linearly with degree of delithiation. The peak temperature of the DSC exotherms shifted to lower temperatures as the degree of delithiation increased. Their results indicate that dried samples (electrolyte removed) released significantly less heat, but quantitative results were not provided.

MacNeil et al. [32] studied the reaction of $Li_xMn_2O_4$ and electrolyte. They found the thermal stability of $Li_xMn_2O_4$ decreased as the concentration of $LiPF_6$ (in EC/DEC) increased. For reaction of 0.1 g of Mn_2O_4 with 0.1 g of electrolyte, they found a heat release of 64 J versus a theoretical (based on complete oxidation of EC) of 263 J; indicating the solvent is not completely oxidized.

The heat of reaction for positive decomposition is coupled with that of solvent oxidation. However, the mechanism is not clear. Positive active material could react directly with solvent, or disproportionate to give off oxygen that reacts with solvent.

3.6. Lithium metal reactions

Little data is available on these reactions. Work by von Sacken et al. [15] found that lithium metal anodes were less stable than lithiated carbon anodes. There is some evidence [26,28] that the electrolyte reaction exhibits a peak at the melting point of lithium (~180 °C). DSC studies with lithium metal and PVDF indicate that this reaction takes place at higher temperatures than the lithiated carbon/PVDF reaction [18,28]. However, this result is likely due to the low surface area of the materials. In a battery, lithium metal and PVDF would be well dispersed and possibly in intimate contact.

Kawamura et al. [43] found using DSC that lithium metal exhibits an exothermic peak with dry electrolytes (1 M $LiPF_6$ in 1:1 PC:DMC or 1:1 EC:DMC or 1:1 EC:DEC) at ~180 °C. They suggest that the SEI layer on lithium protects the metal from reaction until the melting point. Addition of 1 wt.% water decreased the temperature of the exothermic peak to ~140 °C which the authors attribute to a less stable SEI.

3.7. Discharge of the battery releases heat due to entropy changes, overpotentials, and ohmic resistances

The amount of heat released due to entropy changes in lithium-ion cells is small relative to ohmic heating. For example, Kim et al. [31] characterized heat generation of $Li_xMn_2O_4$ spinel in a microcalorimeter. At low rates (<1C) of charge/discharge, the thermal behavior reflected reversible processes. At and above 1C, the thermal behavior was dominated by irreversible processes (ohmic and overpotentials).

3.8. Summary of component studies

Table 1a–d summarizes data on heat release from thermal reactions taking place in lithium-ion cells.

The model requires expressing the heats of reaction in terms of moles. Table 2 summarizes the heats of reactions on a molar basis.

4. Estimation of reaction parameters

All the reactions are assumed to follow an Arrhenius expression for the kinetic rate constant. There is very limited information on activation energies (E_a) and frequency factors (k_0). In order to estimate these values, the following procedure was followed. First, assuming all the reactions are pseudo-first-order,[1] allowed writing a rate expression involving activation energy and frequency factor. This rate expression was used in an energy balance with two unknowns: the activation energy and frequency factor. By, somewhat arbitrarily, specifying the adiabatic self-heating rate as 0.001 °C/min at the onset temperature for thermal runaway (estimated from literature review or guessed, see Table 3), the activation energy and frequency factor could be computed. The results are summarized in Table 3.

These kinetic parameters can be used to simulate DSC and ARC experiments. Figs. 1 and 2 show the simulation results. The DSC curves (Fig. 1) indicate the magnitudes of the heat released per gram of reaction mixture (1:1 molar ratio for binary reactions). The reactions involving lithium metal are more pronounced than the analogous LiC_6 reactions because of the low MW of lithium. The DSC traces suggest a sequence for the reactions, but the ARC simulations more clearly illustrate how the reactions overlap.

The ARC simulations (Fig. 2) indicate the SEI decomposition will begin first at 70 °C. At 85 °C, the lithium/solvent reaction begins and then, at 110 °C the negative/solvent reaction begins. The LiC_6/binder reaction begins at 160 °C but goes at a lower rate than the $NiCoO_2$ decomposition reaction, so by 170 °C the $NiCoO_2$ reaction is taking place at a higher rate than the negative/binder reaction. The solvent decomposition and lithium/binder reactions both begin at 180 °C, but the self-heating rate of solvent decomposition reaction is slightly slower. Finally, at 190 °C decomposition of Mn_2O_4 begins. Because of the overlapping reactions, the role of individual components in thermal runaway is not clear; this is exemplified by the reaction between binder and lithiated carbon.

The PVDF binder reacts only with the negative, if there is negative reactant left after reacting with solvent. Even then, the positive electrode reaction quickly overwhelms the

[1] The assumption of first-order reactions is only made in estimation of parameters. In the battery simulation model calculations, second-order and non-integral order reactions are considered (see Table 4).

Table 1
Summary of reaction parameters

Reference	SEI Reaction		LiC_6/solvent		LiC_6/PVDF	
	Energy (J/g)	Temperature range (°C)	Energy (J/g)	Temperature range (°C)	Energy (J/g)	Temperature range (°C)
(a) Negative electrode (J/g of carbon, fully charged)						
[4]			350	110–150	1500	240–350
[11]			1497	90–290		
[7,12,29]	257	100	1714			
[3]		100			~1100	220–300
[2]	186	130				
[17]			1460	206–215		
[18] ($Li_{0.9}C_6$)			720	110–260	1394	270–400

(b) Positive electrode decomposition (per g of active, fully charged)

Reference	$LiCoO_2$		$LiMn_2O_4$		$Li_xNi_{0.8}Co_{0.2}O_2$	
	Energy (J/g)	Temperature range (°C)	Energy (J/g)	Temperature range (°C)	Energy (J/g)	Temperature range (°C)
[5]					115	175–340[b]
[3]	146	178–250				

(c) Positive/solvent reaction (per g of active)

Reference	$LiCoO_2$		$LiMn_2O_4$		$Li_xNi_{0.8}Co_{0.2}O_2$	
	Energy (J/g)	Temperature range (°C)	Energy (J/g)	Temperature range (°C)	Energy (J/g)	Temperature range (°C)
[4]	450	220–500	450	150–300	600[a]	180–500[a]
[1,6]	381	235			641.7	216
[11]	615	230–300				
[8]	265	170–240				
[2]	625	200–260	350	200–400	1256	200–230[c]
[3]	407	167–250				

(d) Electrolyte (per g of electrolyte)

Reference	Solvent	
	Energy (J/g)	Temperature range (°C)
[9]	~285	250–350
[4]	250	130–220
[11]	155	225–300
[43]	370–530	230–280

[a] $Li_{0.3}NiO_2$.
[b] $Li_{0.5}NiO_2$.
[c] $Li_{0.25}NiO_2$.

Table 2
Selected heats of reactions (per mole)

Reaction	Equation	Literature values (J/g)	g/eq.	J/eq. or J/mol
SEI	**SEI**→ I	186–257	81.2[a]	$1.5–2.1 \times 10^4$
LiC_6/solvent	$\mathbf{LiC_6} + \upsilon_{NS}RS \rightarrow I$	350–1714	81.2[a]	$0.28–1.39 \times 10^5$
LiC_6/binder	$\mathbf{LiC_6} + \upsilon_{NB}B \rightarrow I$	1100–1500	81.2[a]	$0.89–1.2 \times 10^5$
$LiCoO_2$		265–625	195.75	$0.52–1.2 \times 10^5$
$Li_xNi_{0.8}Co_{0.2}O_2$	$\mathbf{NiCoO_2} \rightarrow I + \frac{1}{3}O_2$	600–1256	139.8	$0.8–1.8 \times 10^5$
$LiMn_2O_4$	$\mathbf{Mn_2O_4} \rightarrow I + \frac{1}{2}O_2$	350–450	180.8	$6.3–8.1 \times 10^4$
Solvent decomposition	$\mathbf{S} \rightarrow I$	155–285	100	$1.5–2.9 \times 10^4$
Solvent oxidation	$O_2 + \upsilon_{PS}\mathbf{OS} \rightarrow I$			1.43×10^6[b]

Reactions included in model. I: inert. Mass balance kept on species in bold type.
[a] Assuming 330 mAh/g.
[b] For dimethylcarbonate (from CRC Handbook, 63rd ed.).

Table 3
Estimated kinetic parameters

Reaction	T_{onset} (°C)	T_{peak} (°C) @ 10 °C/min	H/C_p (K)	E_a (J/eq.)	k_0 (s^{-1})
$Li + \upsilon_{LIB}B \rightarrow I$	180	280	1.93×10^4	2.86×10^5	1.917×10^{25}
$Li + \upsilon_{LIS}RS \rightarrow I$	85	180	1.02×10^4	2.05×10^5	9.41×10^{21}
$LiC_6 + \upsilon_{NB}B \rightarrow C_6 + I$	160	300	3.71×10^3	1.67×10^5	1.79×10^{13}
$LiC_6 + \upsilon_{NS}RS \rightarrow C_6 + I$	110	200	9.81×10^2	2.0×10^5	1.95×10^{20}
$Li_{0.5}NiCoO_2 \rightarrow I + \frac{1}{3}O_2$	165	225	5.30×10^2	3.94×10^5	7.25×10^{39}
$Mn_2O_4 \rightarrow I + \frac{1}{2}O_2$	190	300	7.23×10^2	2.18×10^5	1.06×10^{18}
$S \rightarrow I$	180	250	1.91×10^2	2.74×10^5	5.14×10^{25}
$SEI \rightarrow I$	70	110	1.43×10^2	2.81×10^5	7.88×10^{36}

H: heat of reaction, C_p: heat capacity.

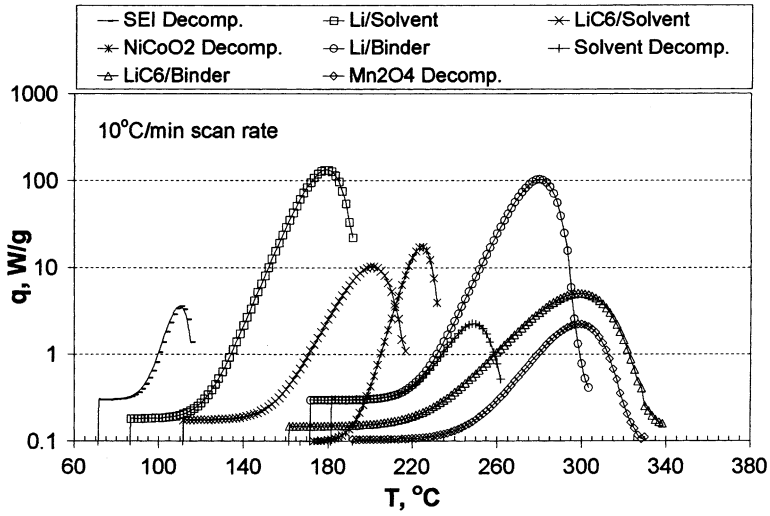

Fig. 1. Simulated DSC experiments for cell components.

negative/binder reaction, so it is not clear that the binder reaction is important. If the heat generated from the SEI and LiC_6/solvent reactions, and perhaps, electrical heating, is sufficient to initiate decomposition of the positive, then the reactivity of the binder with Li may be a moot point.

5. Base case development

Two lithium-ion chemistries are in competition for use in hybrid electric vehicles and 42-V batteries: $LiNi_zCo_{1-z}O_2$ [22] and $LiMn_2O_4$ [21]. $LiNi_zCo_{1-z}O_2$-cathodes provide

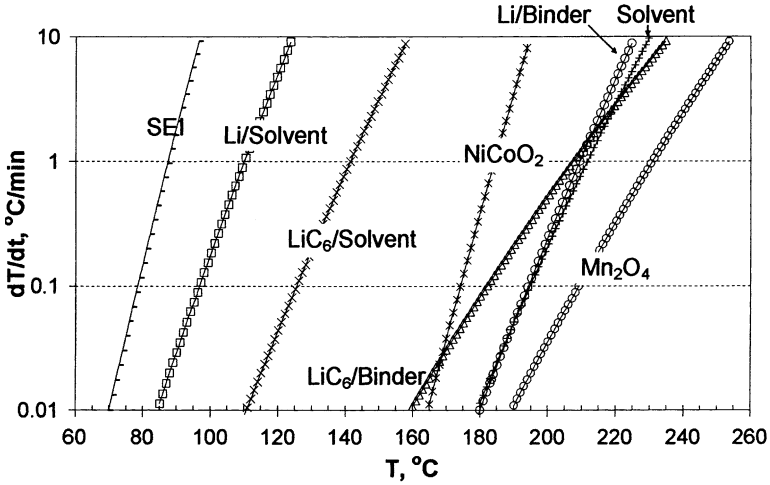

Fig. 2. Simulated ARC experiments.

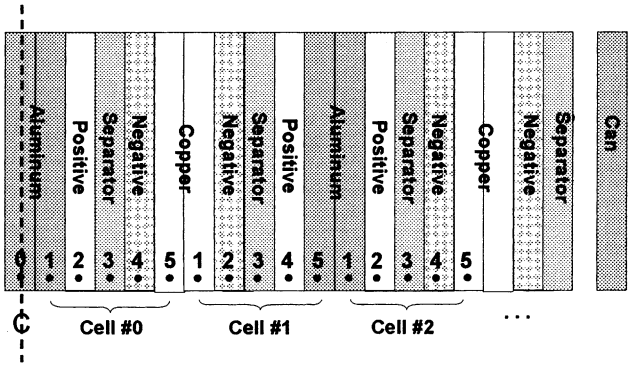

Fig. 3. Geometry of cell.

better life, but are more expensive than $LiMn_2O_4$-based cathodes. To model the abuse behavior of these chemistries, some educated guesses must be made as to the internal design of the corresponding batteries. Specifically, the dimensions of the electrodes, collectors, and separator must be known, as well as the compositions. With these parameters, a unit cell (see Fig. 3), consisting of Al collector, positive, separator, negative, Cu collector, can be specified. This unit cell can be used to develop model parameters. Given the thickness of the prismatic cell, and the unit cell properties (see Table 7), the simulation model can be specified.

Given the quantities and heat capacities of the materials present in each type of cell, and the heats of reaction, the maximum temperature rise for the overall battery due to each reaction can be estimated. This calculation assumes the heat of reaction is uniformly distributed throughout all components of the battery and so does not account for local heating effects (“hotspots”). Further, discharge and charge conditions will be different. On discharge the active material is limited by the initial state of charge, but, on charge, lithium metal is deposited and the amount of positive active is increased (up to a certain point). Figs. 4 and 5 illustrate the maximum temperature rise possible due to each exothermic process in the cell. The maximum temperature rise for each process during discharge could correspond to an oven test, short-circuit, crush, or nail test; whereas, the maximum temperature rise for each process during charge could correspond to an overcharge test.

Both chemistries exhibit similar behavior. The temperature rise due to SEI decomposition is very small (<2 °C). The negative/solvent reaction can raise the cell temperature ~100 °C. The biggest difference between the two chemistries is on charge. Since the manganese oxide cannot be overcharged (excess charge goes to solvent oxidation), while the nickel cobalt oxide electrode can be further delithiated, the manganese cell generates a greater temperature rise due to solvent oxidation. Also on charge, reactions with lithium metal lead to significant temperature rises.

On discharge, if all the electrical energy went to cell heating, the cell temperature would increase well above 500 °C.

The solvent oxidation and positive active decomposition reactions should be considered as coupled (oxygen from the positive oxidizes solvent). Solvent oxidation causes a significant temperature rise (>100 °C), but this must be taken with some skepticism, as some data suggest the heat released from the positive/solvent reaction is much less than that calculated from combustion of solvent with oxygen released from the positive.

The temperature rise due to the negative/binder and negative/solvent are similar, even though the negative/binder

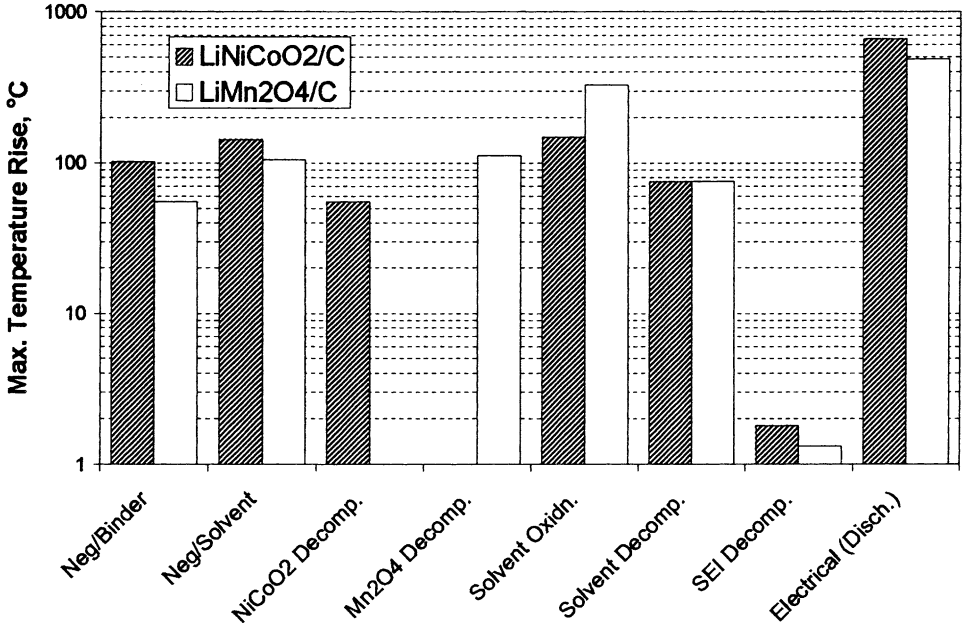

Fig. 4. Maximum temperature rise due to exothermic processes during discharge.

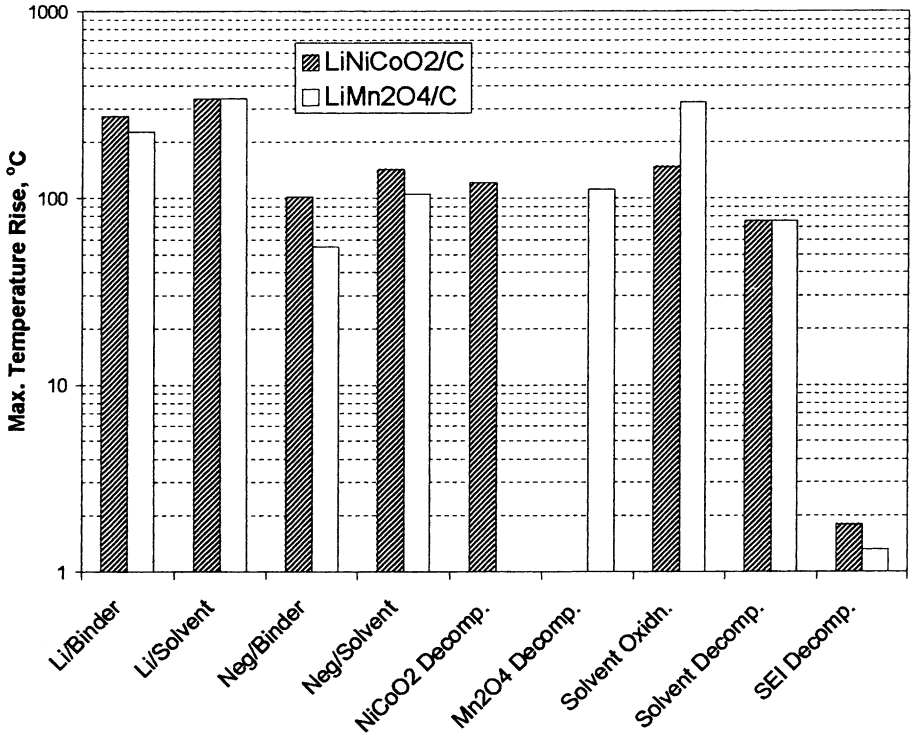

Fig. 5. Maximum temperature rise due to exothermic processes during charge.

reaction is much more exothermic because there are much fewer moles of binder than solvent. A key question is the relative rates of the negative/solvent and negative/binder reactions. While published worked has shown that fluorinated binders react more exothermically with lithiated carbon than non-fluorinated binders [10], the relative rates of the negative/binder and negative/solvent reactions have not been clearly addressed. Biensan et al. [4] do give a plot of heat release versus time for these reactions, but an isotherm of 700 °C is selected and the time scale does not resolve the two processes.

6. Survey of thermal modeling of lithium-ion cells

A significant amount of work has been carried out to develop mathematical models for the thermal design of lithium-ion cells; only a few representative papers will be described here. Chen and Evans [35] considered the problem of heat generation in a prismatic stack of lithium-ion cells using a simple energy balance:

$$\rho C_p \frac{\partial T}{\partial t} = k_x \frac{\partial^2 T}{\partial x^2} + k_y \frac{\partial^2 T}{\partial y^2} + k_z \frac{\partial^2 T}{\partial z^2} + q \tag{7}$$

where T is the temperature; t time; ρ the cell density; C_p the heat capacity; k a thermal conductivity; x, y, and z represent spatial dimensions; and q is the generation rate. The heat generation rate was taken as uniform throughout the cell and determined from experiments with actual cells. The thermal conductivity was computed by averaging reported and estimated properties of the cell components. The calculations indicate that, even for large cells (20 cm × 20 cm × 20 cm), the cell temperature would not reach extreme values, nor would the temperature gradients be large. Abuse behavior was simulated by setting the internal heat generation rate at the center of the cell to a high value for a short time and following the temperature profile with time; these calculations indicated that thermal runaway could occur in the event of a localized internal short-circuit. Kanari et al. [36] used an approach similar to Chen and Evans [35], but considered a cylindrical cell and compared their results to experimental data obtained with a Sony 18,650 cell. The heat generation rate (q) was computed based on the following equation:

$$q = -I(E_{\text{emf}} - V) + I\left(T\frac{\partial E_{\text{emf}}}{\partial T}\right) \tag{8}$$

where I is the cell current, E the cell voltage, and E_{emf} the equilibrium cell voltage. The computed temperatures of the can at both ends and at the mid-point of the tube agreed well with experimental data during discharge and charge (within 2 K). Al Hallaj et al. [33] developed a simplified one-dimensional model that gave good agreement with experimental measurements of the temperature of a Sony 18,650 cell. They used the model to estimate the thermal behavior of larger (10–100 Ah) cells and found that at high discharge rates (1C) the internal temperature increased by ∼60 °C. Sato [37] compared experimental and model predictions for the temperature rise during discharge of an 80 Ah Li-ion cell and obtained good agreement. Most recently, Funahashi et al. [38] used a model similar to that of Kanari et al. [36] to

compare with actual data for a 250 Wh cell. They found excellent agreement between measured and computed surface temperatures at a 1*C* discharge up to ~60% DOD (~25 °C temperature rise); at higher DOD the model over-predicted the temperature rise (model estimated ~36 °C increase versus measured ~30 °C). The discrepancy is most likely because the *I*/*E* data obtained from small cell testing does not accurately represent the large cell *I*/*E* behavior. The large cell heats up as it discharges and the small cell *I*/*E* data does not reflect this. Since polarization decreases with increasing temperature (as both mass transport and reaction kinetics increase with temperature) the large cell generates less heat than the model predicts. By modeling the polarization due to mass transport and charge transfer, a more accurate estimate of the thermal behavior might be obtained. Models have been developed that include estimates for ohmic and polarization voltage losses and these models have been demonstrated to give good predictions of current–voltage behavior of small lithium-ion cells [39], however, comparisons with thermal behavior have not yet been reported.

The response of batteries to oven heating (an abuse test) has been predicted using a model that accounts for the kinetic behavior of the positive and negative electrodes [37]. Hatchard et al. [12] obtained reasonable agreement between model calculations and experimental oven tests for 18,650-size cells. They used the model to predict the effect of increasing the radius of a cylindrical cell and of increasing the thickness of a prismatic cell. In both cases, they found a critical size at which thermal runaway would result.

7. Model development

For simplicity, a cell is modeled as a slab consisting of layers of various materials (see Fig. 3). Only one dimension is considered (*x*-direction), the slab is considered uniform in the *y* and *z* directions. By symmetry, only half of the cell is considered. The origin of the coordinate system is at the center of the cell. Using a control volume approach [40], mass and energy balances are carried out for each layer of the cell. The positive, separator, and negative layers are composites. The electrodes consist of active material, electrolyte, binder and inert materials, while the separator consists of electrolyte and inert material; shutdown (melting) of the separator is not considered in the model. The boundary condition at the centerline is that the heat flux is zero, and the boundary condition at the can, is that heat can transfer by convection and radiation. Table 4 summarizes the kinetic equations, while Table 5 lists the mass balance equations and Table 6 lists the source terms in the energy balance (see Eq. (7)). The set of differential equations was solved using the IDA routine of Hindmarsh and Taylor [41].

The forms of the kinetic expressions in Table 4 are explained as follows. The rates of the positive (R_P), solvent (R_S) and SEI (R_{SEI}) decomposition reactions are all taken as

Table 4
Kinetic equations

Reaction	Equation
Positive decomposition	$R_P = k_P m_{PO}$
Solvent decomposition	$R_S = k_S c_S$
Negative solvent	$R_{NS} = L_N r_{NS}, \quad r_{NS} = \frac{k_{NS}}{L_E} x_s a_{s,N} l_N w_N r_S \varepsilon_N,$ $L_E = L_E^0 + \frac{m_E}{m_N a_{s,N} \rho_E}$
Negative binder	$R_{NB} = k_{NB} a_{s,N} w_N l_N x_s \upsilon_N (1-\varepsilon_N) c_N^0 w_B$
Li diffusion in negative	$N_N = -a_{s,N} l_N w_N k_{m,N} c_N^0 (x_s - x_b)$
SEI decomposition	$R_{SEI} = k_{SEI} m_E$
Lithium solvent	$R_{LiS} = k_{LiS} L_N \varepsilon_N \frac{k_{Li} m_{Li}}{1 + k_{Li} m_{Li}} c_S$
Lithium binder	$R_{LiB} = k_{LiB} \frac{k_{Li} m_{Li}}{1 + k_{Li} m_{Li}} \frac{w_B l_N}{B_{MW}}$

Table 5
Mass balance equations

Species	Symbol	Mass balance
Positive active in oxidized state	m_{PO}	$\frac{dm_{PO}}{dt} = -R_P + \frac{i}{F}$
Positive active in reduced state	m_{PR}	$\frac{dm_{PR}}{dt} = -\frac{i}{F}$
Solvent in the positive, negative, and separator	c_S	$\frac{dc_S}{dt} = -R_S$
Oxidizable solvent in the positive	c_O	$\frac{dc_O}{dt} = \frac{-\upsilon_{PS} R_P + \upsilon_S (i_{OC}/F)}{\varepsilon_P L_P}$
Reducible solvent in the negative	c_R	$\frac{dc_R}{dt} = -\frac{\upsilon_{NS} R_{NS} + \upsilon_{LiS} R_{LiS}}{\varepsilon_N L_N}$
Intercalated lithium in negative	x_b	$\frac{dx_b}{dt} = -\frac{N_N}{L_N (1-\varepsilon_N) \upsilon_N c_N^0}$
SEI material	m_E	$\frac{dm_E}{dt} = -R_{SEI}$
Li metal	m_{Li}	$\frac{dm_{Li}}{dt} = -R_{LiS} - R_{LiB} + \frac{i_{Li}}{F}$
Binder in negative	w_B	$\frac{dw_B}{dt} = -\frac{B_{MW}}{l_N} (R_{LiB} + R_{NB})$

Table 6
Energy balance source terms

Test or element	Equation
Oven	$S_{ohm} = 0$
Short	$S_{ohm} = i^2 \frac{L_i}{\sigma_i}, \quad i = F k_d x_b$
Overcharge	$S_{ohm} = i_{OC}^2 \frac{L_i}{\sigma_i}$
Nail	$S_{ohm} = i^2 \frac{L_i}{\sigma_i} + i_{nail}^2 \frac{L_i}{\sigma_{nail}}, \quad i_{nail} = \frac{\sum i}{N_{shorted}}$
Crush	$S_{ohm} = i^2 \frac{L_i}{\sigma_i} + i_{crush}^2 \frac{L_i}{\sigma_{cell}}, \quad i_{crush} = \frac{\sum i}{N_{crushed}}$
Collector	$S = S_{ohm}$
Positive active	$S_P = i E_{pos} + R_P H_P + L_{pos} R_S H_S + \frac{i_{oc}}{F} H_P + S_{ohm}$
Separator	$S_S = i^2 R_{sep} + L_{sep} R_S H_S + S_{ohm}$
Negative active	$S_N = i E_{neg} + R_{NS} H_{NS} + R_S H_S + R_{NB} H_{NB} + R_{SEI} H_{SEI} + R_{LiS} H_{LiS} + R_{LiB} H_{LiB} + S_{ohm}$

Table 7
Physical properties of base case unit cells [20,42]

	C_{base}		M_{base}	
	$LiNiCoO_2$	Graphite	$LiMn_2O_4$	Graphite
Weight fraction				
Active	0.84	0.92	0.87	0.94
Binder	0.06	0.08	0.06	0.06
Carbon black	0.1	0	0.07	0
Solids density (g/cm^3)	4.584	2.211	4.202	2.223
Heat capacity (J/(g K))	0.651	0.720	0.672	0.641
Thermal conductivity (W/(cm K))	0.061	0.063	0.062	0.065
Apparent density (g/cm^3)	2.75	1.08	2.62	1.08
Porosity	0.400	0.512	0.377	0.514
Electrolyte-filled				
Density (g/cm^3)	3.233	1.697	3.074	1.701
Heat capacity (J/(g K))	0.823	1.113	0.839	1.064
Thermal conductivity (W/(cm K))	0.037	0.032	0.039	0.033
Weight fraction				
Electrolyte	0.149	0.364	0.148	0.365
Solids	0.851	0.636	0.852	0.635

Table 8
Design parameters for base case unit cells

Parameter	$NiCoO_2$/C cell		Mn_2O_4/C cell	
	$NiCoO_2$	Carbon	Mn_2O_4	Carbon
Active				
Capacity (mAh/g)	160	330	115	330
Capacity (mAh/cm^2)	1.4784	1.4784	1.2006	1.2006
Loading (mg/cm^2)	11	4.87	12	3.87
Coat thickness (μm)	40.0	45.1	45.8	35.8
Separator thickness (μm)	25.4	25.4	40.0	40.0
Separator porosity (%)	40.0	40.0	40.0	40.0
Collector thicknes/2 (μm)	10.0	5.0	10.0	5.0
Unit cell thickness (μm)	125.5		136.6	
Total area (cm^2)	7730.4		4997.5	
Unit cell area (cm^2)	23.78	23.78	20.20	20.20
Overall thickness (cm)	4.08		3.38	
Overall volume (cm^3)	97.01		68.29	
Number of unit cells	325	325	247	247
Coating weight (g)	85.0	37.6	60.0	19.3
Coating volume (cm^3)	30.9	34.9	22.9	17.9
Active weight (g)	71.43	34.63	52.17	18.18
Binder weight (g)	5.10	3.01	3.60	1.16
Carbon weight (g)	8.50	0.00	4.20	0.00
Electrolyte weight (g)	14.93	21.52	10.40	11.12
Collector weight (g)	20.78	34.32	13.43	22.19
Electrode weight (g)	120.75	93.49	83.81	52.65
Separator polymer (g)	10.84		11.03	
Separator electrolyte (g)	9.42		9.60	
Wet separator weight (g)	20.26		20.63	
Can weight (g)	3.77		3.20	
Jellyroll weight (g)	234.50		157.08	

first-order; this seems reasonable given the limited information available about them. The rate of the negative solvent reaction (R_{NS}) is taken to be inversely proportional to the amount of SEI material and proportional to the surface area of the negative and the surface concentration of lithiated carbon; this type of expression is similar to that used by Richard and Dahn [7]. The surface concentration of lithiated carbon was determined using a lumped mass balance and the flux expression given in Table 4 for lithium-ion diffusion in carbon. The reaction of lithiated carbon and binder was taken to be proportional to the amount of binder and the surface concentration of lithium. The reactions with metallic lithium were taken as first-order in solvent or binder, and to depend only slightly on the amount of lithium. The k_{Li} parameter was set to a large value, to effectively make the term $k_{Li}m_{Li}/(1 + k_{Li}m_{Li})$ equal to unity when $m_{Li} \gg 0$, and zero when $m_{Li} = 0$.

The physical properties of the materials commonly found in lithium-ion cells were taken from the literature [19]; Table 7 lists the physical properties used and Table 8 details the design parameters for the base case cells.

8. Case studies

8.1. Oven test

For a 175 °C oven test, Fig. 6 shows how the temperature profile develops in the battery over time. The figure shows the temperature distribution in one half of the battery (the other half is the same by symmetry); the core temperature is shown on the left and the can temperature on the right. As the battery heats up, the temperature is highest at the can surface and steadily decreases toward the core (see 4999.69 s). As the exothermic reactions are activated and start to release heat, the interior temperature of the battery increases, and the temperature reaches a maximum at the core and steadily decreases toward the wall. At 5839 s, thermal runaway ensues starting at the innermost cell of the battery. The contribution of the various reactions can be visualized with the aid of Fig. 7. This figure shows the cumulative energy released from each reaction as a function of time. The cause

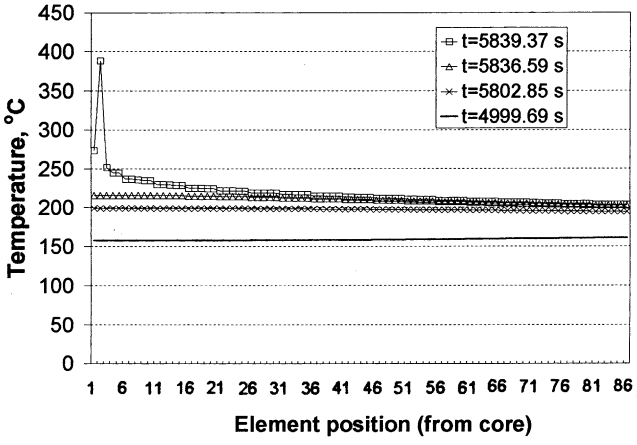

Fig. 6. Temperature profiles for oven test (175 °C) with $NiCoO_2$ case.

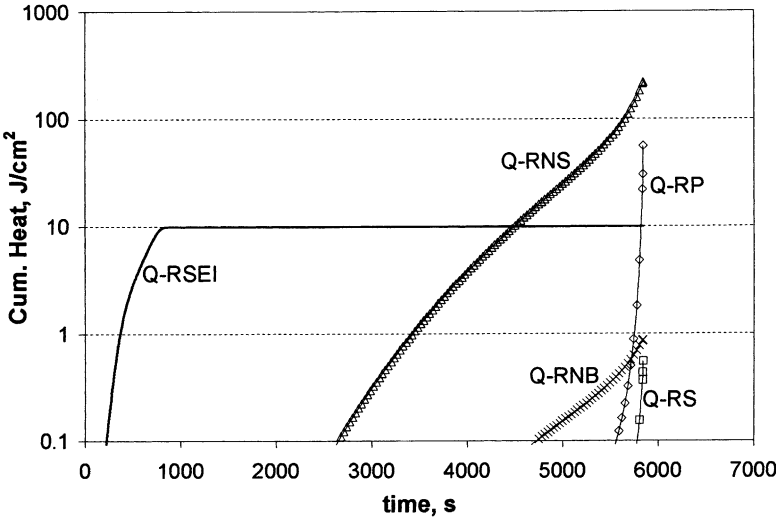

Fig. 7. Cumulative energy vs. time for $NiCoO_2$ case (175 °C oven).

of the runaway can be associated with the negative/solvent reaction (Q-RNS), the positive decomposition reaction (Q-RP), the solvent decomposition reaction (Q-RS), and possibly the negative/binder reaction (Q-NB).

Since the value for the negative surface area used to obtain Figs. 6 and 7 is somewhat low (0.8 m^2/g), cases were run with higher values (2.4 and 4.8 m^2/g). The temperature profiles at the start of thermal runaway are shown in Fig. 8. As the surface area of the negative active material increases, the time for thermal runaway to initiate decreases, and the position in the cell where thermal runaway initiates moves closer to the wall. These results can be explained as follows. When the negative area is low (0.8 m^2/g), the negative/solvent and negative/binder reactions rates initially generate heat at a rate low enough that it can be dissipated through the can wall. This sets up a temperature profile with the maximum temperature at the core. As the temperature increases, the rate of heat generation exceeds the rate of heat dissipation and runaway ensues starting at the core (highest temperature). Increasing the negative area increases the rate

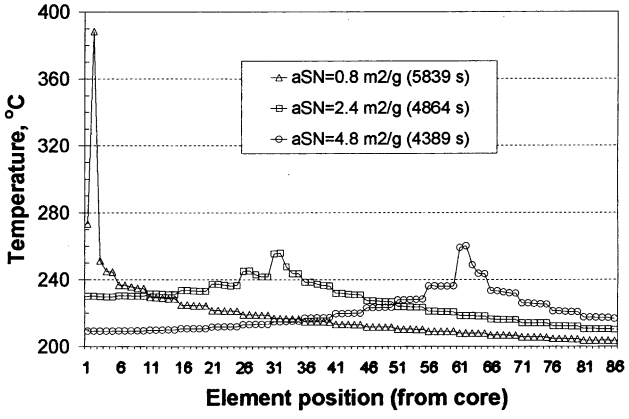

Fig. 8. Temperature profiles for $LiNiCoO_2$ with varying negative active areas (175 °C oven).

of heat release from the negative/solvent and negative/binder reactions. In this case, just before thermal runaway, the temperature profile is such that the highest temperature is at the can wall. So the heat generation rate is highest at the can wall and lowest at the core. Since the heat generated nearest the can wall is dissipated by convection, the temperature near the can wall becomes lower than the interior. The interior temperature rises due to heat generation and the temperature profile shows a maximum because the rate of heat generation is decreasing toward the core (lowest temperature). In all cases, the contribution of the negative/binder reaction appears small relative to that of the negative/solvent reaction.

To see if the negative/binder reaction contributed to thermal runaway, a case was run using a negative area of 4.8 m^2/g and setting the enthalpy for the negative/binder reaction to zero. The results were almost identical to the case where the enthalpy of the negative/binder reaction was considered (without the binder reaction, the time to runaway increased by only 4.5 s). Thus, even though some energy is released by the negative/binder reaction, it is insignificant compared the positive and solvent decomposition reactions. Under the conditions described here, the binder does not play a role in thermal runaway.

The Mn_2O_4 cell differs from the $NiCoO_2$ cell in several important ways. Mn_2O_4 is more thermally stable than $NiCoO_2$. The Mn_2O_4 cell is thinner, so better able to dissipate heat. The Mn_2O_4 cell contains less binder in the negative (6 wt.% versus 8 wt.% for the $NiCoO_2$ cell). The difference in the cells reflects differences observed in commercial cell designs. The results of a 175 °C oven test for the Mn_2O_4 cell are shown in Figs. 9 and 10. Thermal runaway occurs in the following manner (see Fig. 10). The SEI reaction contributes a small amount of heat, but it overshadowed by the negative/solvent reaction. The solvent decomposition reaction, once activated, proceeds to completion. The negative/binder reaction is inhibited by the slow

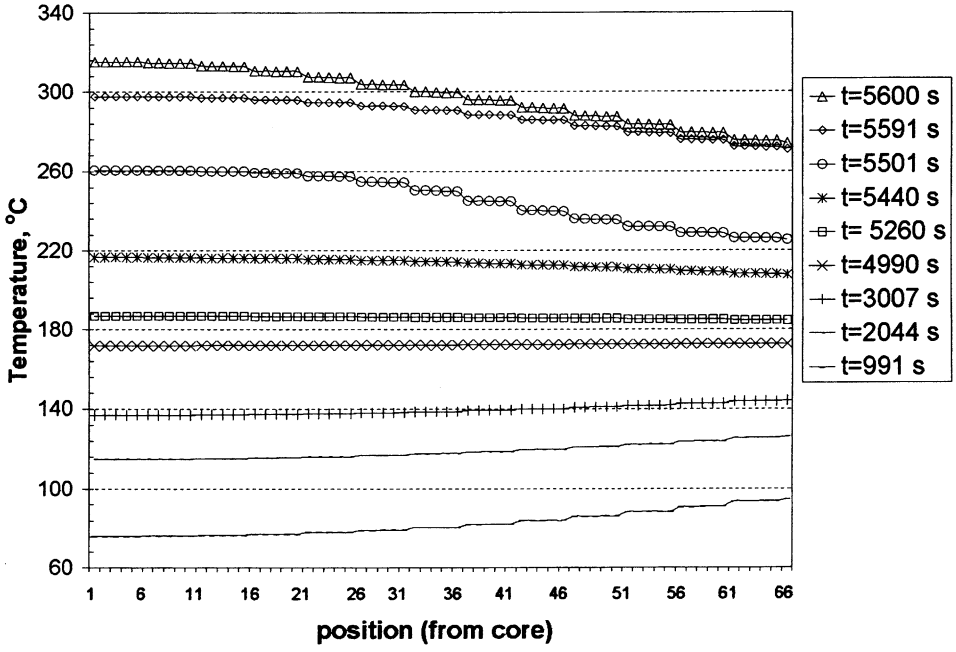

Fig. 9. Temperature profiles for oven test (175 °C) with Mn_2O_4 case.

rate of lithium diffusion out of the negative electrode and does not release a significant amount of energy. Thermal runaway results from the positive electrode decomposition reaction.

In the Mn_2O_4 simulations, the solvent decomposition reaction contributes a significant amount of energy. If a lower porosity negative electrode is used (~25% versus 50% for base case), the amount of solvent will be significantly reduced. Figs. 11 and 12 show the results of reducing the negative porosity and using a higher value for the mass-transfer coefficient of lithium diffusion in the negative (10^{-6} cm/s versus 10^{-7} cm/s for base case). In this case the battery reaches a maximum temperature of only ~242 °C. The SEI decomposition, solvent decomposition, negative/binder, and negative/solvent reactions proceed to completion without raising the cell temperature to the point where the positive electrode reaction runs away. However, thermal runaway does result if the surface area of the negative electrode is increased to 4.8 m^2/g, because the cell temperature rises above 265 °C, and the positive electrode decomposition reaction takes off.

These simulations indicate the negative/binder reaction is relatively unimportant in the oven test. The binder must compete with the more facile solvent reaction to react with the negative electrode. Based on the understanding generated by these simulations, it is possible to predict that the binder reaction could be important in situations where the amount of solvent is limited (low porosity electrodes) and a

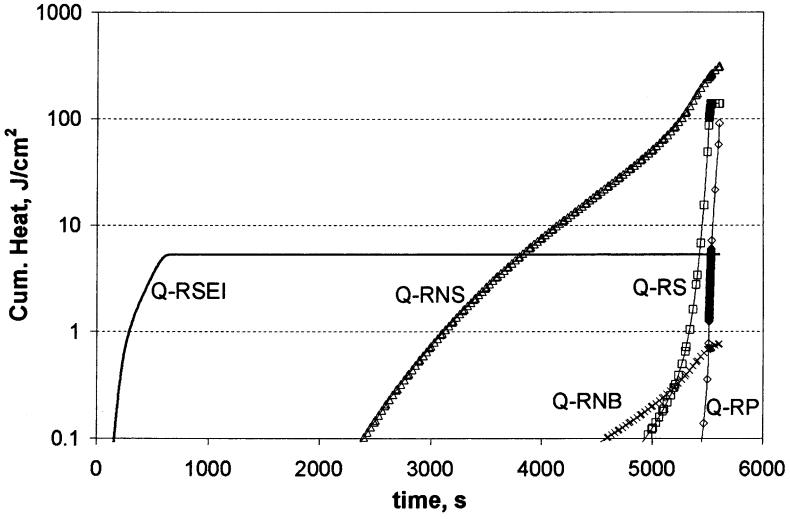

Fig. 10. Cumulative energy generated vs. time for Mn_2O_4 cell (175 °C oven test). Negative area 4.8 m^2/g.

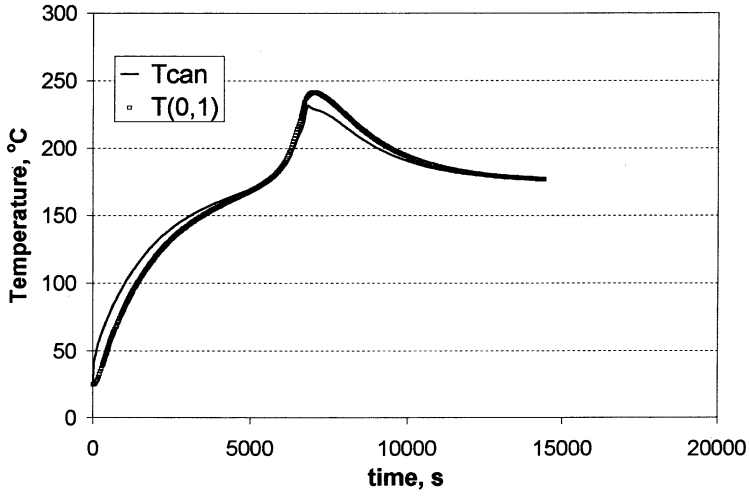

Fig. 11. Temperature versus time for Mn_2O_4 cell (175 °C oven). Negative porosity ~25%, $k_{mn} = 10^{-6}$ cm/s.

high binder loading (10 wt.%) is used. However, both of these conditions are contrary to producing high-rate negative electrodes.

8.2. Short-circuit test

In this test, the possibility exists for electrical heating to raise the temperature of the cell to the point where thermal runaway initiates. The current is limited by diffusion of lithium in the negative, and so either increasing the mass-transfer coefficient for lithium in the negative or increasing the surface area of the negative allows for higher currents and so more rapid heating of the battery. Despite the rapid heating, the positive decomposition reaction is still responsible for thermal runaway. Increasing the mass-transfer coefficient with the negative area set to 4.8 m^2/g reduces the time to thermal runaway to ~13.5 s, but does not change the mechanism for thermal runaway.

As in the oven test, thermal runaway in the short-circuit test is a result of activating the positive decomposition reaction by heating the battery to a high temperature. However, in the short-circuit test, the battery can be heated much more rapidly by irreversible heat generated from passing current through the electrodes. This rapid heating sets up a steep temperature profile with the highest temperature at the core, where the positive decomposition reaction can be activated before the other exothermic reactions (such as the solvent reactions) have progressed significantly. This contrasts with the oven test, in which the battery heats up much more slowly, allowing the solvent reactions to progress significantly before the positive electrode is activated. Thus, with the $NiCoO_2$ cell, the binder plays an even less important role in thermal runaway during the short-circuit test than the oven test.

With the manganese cell, the positive decomposition reaction takes place at a higher temperature than in the

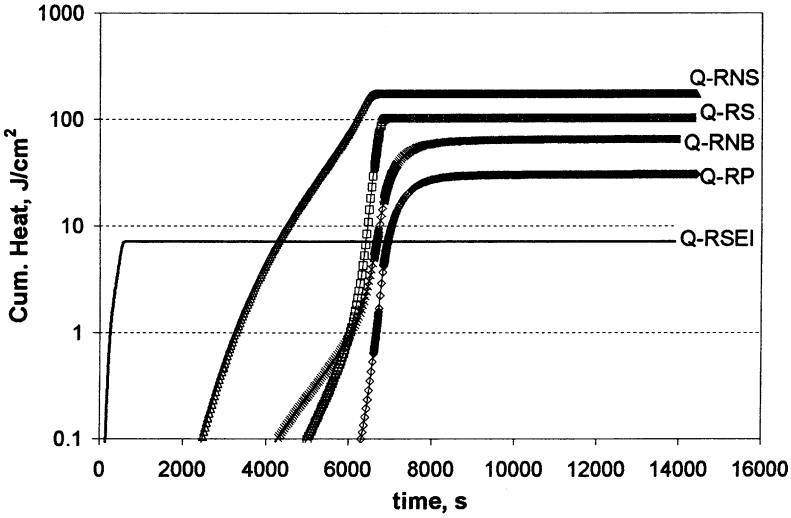

Fig. 12. Cumulative energy versus time for Mn_2O_4 cell (175 °C oven). Negative porosity ~25%, $k_{mn} = 10^{-6}$ cm/s.

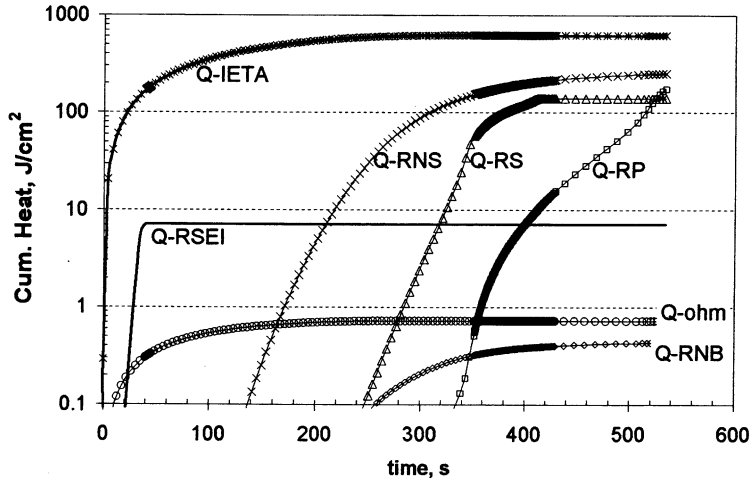

Fig. 13. Cumulative energy versus time for short-circuit test with Mn_2O_4 cell. Mass-transfer coefficient for Li in negative 10^{-7} cm/s and negative area 4.8 m^2/g.

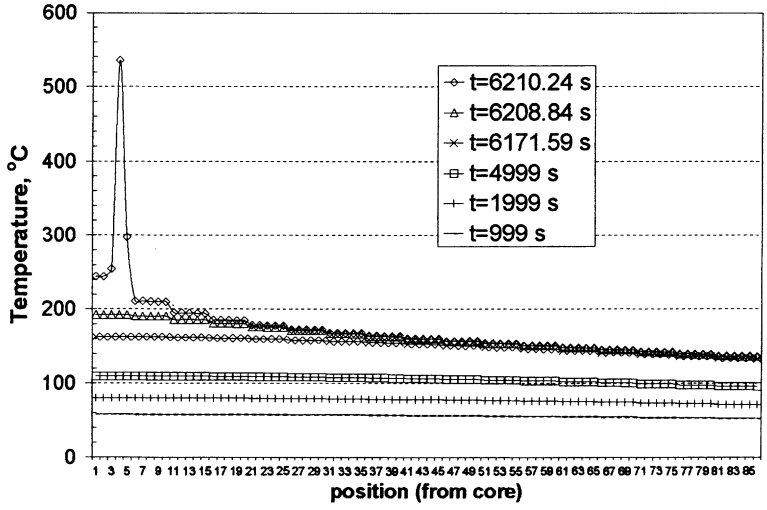

Fig. 14. Temperature profiles for $NiCoO_2$ overcharge test.

$NiCoO_2$ cell, so the solvent reactions have more time to proceed (see Fig. 13). Discharge of the negative and reaction of lithiated carbon with solvent deplete the negative, so the binder reaction takes place to only a very limited extent. Still, the cell goes into thermal runaway due to activation of the positive decomposition reaction.

As in the oven test, the binder does not compete effectively with solvent to react with lithiated carbon, and so plays a limited role in the thermal runaway behavior.

8.3. Overcharge test

Overcharging a lithium-ion battery can lead to lithium metal formation which opens the possibilities for further reactions with the solvent and binder.

The temperature profiles for an overcharge test (1 mA/cm^2, ~C/1.7 rate) with the base case $NiCoO_2$ battery are shown in Fig. 14 and the cumulative energy source terms in Fig. 15. The cell heats up slowly for the first ~5400 s, at which point the electrodes are fully charged and the reactions shift from intercalation at the negative to deposition of lithium metal, and from lithium de-intercalation at the positive to oxidation of solvent. The solvent oxidation

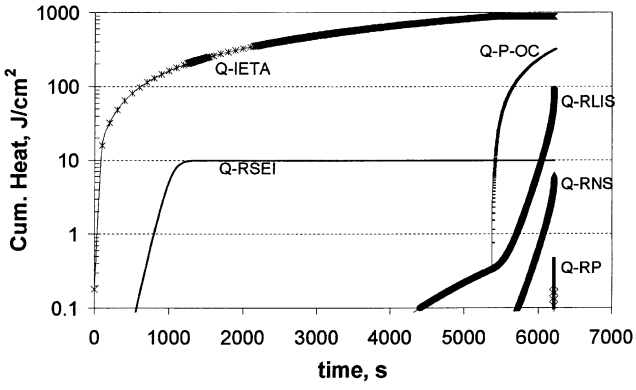

Fig. 15. Heat source terms for $NiCoO_2$ overcharge test.

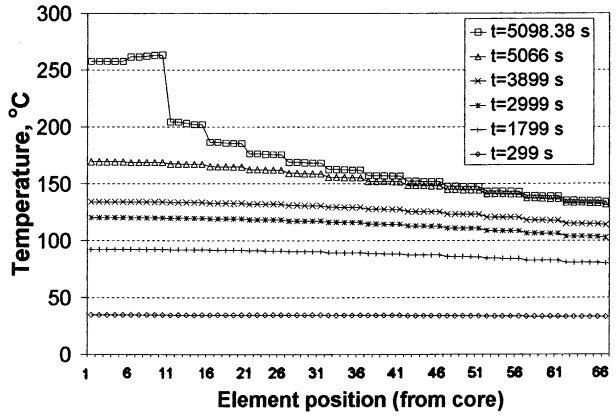

Fig. 16. Temperature profiles for Mn_2O_4 overcharge test. Negative area 4.8 m^2/g.

reaction due to overcharge (Q-P-OC term in Fig. 15) generates heat at a much higher rate than the irreversible heating due to the intercalation reactions. As the temperature rises, first the lithium/solvent reaction, then the negative/solvent reaction become activated, and thermal runaway occurs. Unfortunately, the simulation fails at this point because the gradients become too steep to follow. When thermal runaway occurs, neither the lithium/binder reaction nor the positive decomposition reaction are contributing significant energy. Runaway is mainly due to metallic lithium reacting with solvent.

An overcharge test with the base case Mn_2O_4 cell (1 mA/cm^2, ~C/1.6 rate) yields similar results as with the $NiCoO_2$ battery (see Figs. 16 and 17). At about 900 s, the positive electrode is fully charged and the reaction shifts to solvent oxidation. The solvent oxidation reaction heats the battery and activates the lithium/solvent reaction. This further increases the rate of battery heating and activates the negative/solvent reaction. With thermal runaway well in progress, the solvent decomposition and lithium/binder reactions are activated. To verify the binder plays no role, the simulation was repeated with the enthalpies of the binder

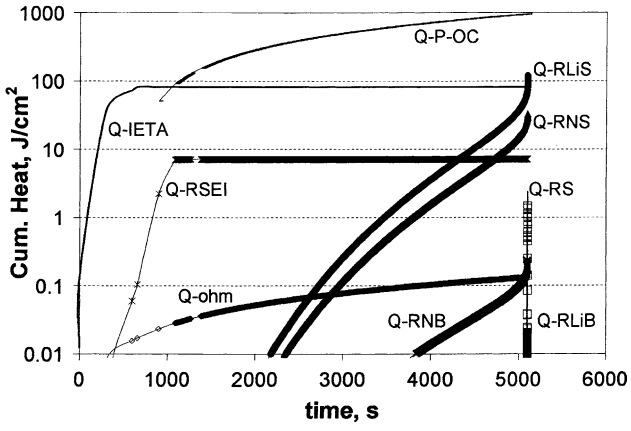

Fig. 17. Heat source terms for Mn_2O_4 overcharge test. Negative area 4.8 m^2/g.

reactions set to zero, and virtually identical results were obtained.

The major experimental observation with the overcharge test is that runaway is sensitive to the charging current. The simulation model shows the same behavior. A simulation run (Mn_2O_4 cell) with a charging current of 0.5 mA/cm^2 does not result in thermal runaway.

If the solvent is depleted, then the binder might play a role. The stoichiometric numbers for the electrolyte/lithium and electrolyte/binder reactions were changed from 0.5 to 2.5 to exaggerate the effect. However, the battery did not get hot enough to activate the binder reactions.

8.4. Nail test

This model, being one-dimensional, can only very crudely approximate the nail test. In this model, the heat released from the nail is instantaneously distributed in the plane perpendicular to the nail movement. In an actual nail test, a local hotspot could form at a particular place in the plane of the battery. A hotspot will form because the heat generated in the nail cannot be dissipated as fast as it is generated even though the thermal conductivity of batteries is typically 10× higher in the plane of the electrodes (due to the metal current collectors) than in the direction the nail penetrates [20]. To simulate a hotspot, since the model does not account for thermal gradients in the plane of the electrodes, the heat generation in the nail was set to a large value. If the nail moves at 8 cm/s, all the cells are rapidly shorted and the results are similar to a short-circuit test; thermal runaway starts at the innermost cell and is due to the positive decomposition reaction. If a much lower nail speed (0.01 cm/s) is used, thermal runaway initiates at the outermost cell; the outermost cell heats up from the current flowing through the nail, which activates the positive decomposition reaction.

8.5. Crush test

In practice, this test is carried out in a variety of ways. The cell can be crushed with a round bar until the cell voltage drops to a low value, or the cell can be crushed by a certain fraction of its thickness (for example, to 50% of its original thickness). To simulate the effect of crush, one or more cells is shorted so that the current generated by the battery flows through those cells. As with the simulated nail test, this simulation suffers by using a one-dimensional model. In reality, the short formed from a crush would be localized to a spot on the electrode while the one-dimensional model must assume the short is uniformly distributed across the plane of the electrode. Since Joule heating is inversely proportional to the area traversed by the current, the one-dimensional model vastly underestimates the amount of heat generated.

Setting the model so that the innermost cell is shorted gives results almost identical to those of a short-circuit test. The battery heats up due to overpotential losses at the

electrodes and activates the negative/solvent reaction. This further heats the battery, activating the positive decomposition reaction and causing thermal runaway.

9. Conclusions and recommendations

The simulations indicate that the negative electrode binder plays a relatively unimportant role in thermal runaway. The amount of binder is limited, and the binder reaction must compete with the more facile solvent reaction for lithiated carbon. Reactions involving lithiated carbon are somewhat hindered because the lithium must diffuse through the solid carbon to react at the surface. When the battery is overcharged, substantial amounts of lithium metal can form. The lithium may be in intimate contact with the binder and can react directly without being hindered by solid-state diffusion. Still, the solvent reaction is preferred and can induce thermal runaway without the aid of the lithium/binder reaction.

The short-circuit test, and especially the nail and crush tests, can cause rapid and localized heating of the battery. This localized heating results in high temperatures that activate all the chemical reactions in the cell. However, since the relative rates of the reactions do not change, the binder reaction still plays a minor role.

The simulations reported here were unable to rationalize the experimental observation that fluorinated binders fail in the nail test above 4.0 V, whereas non-fluorinated binders pass the nail test up to 4.3 V [4]. One possibility is that at very high rates, the binder/negative reaction overtakes that of the electrolyte/negative reaction. Also, the simulations do not account for the possibility that the battery can eject electrolyte. If the electrolyte is displaced, then it would no longer compete with the binder to react with lithium, and the binder reaction could take on greater significance.

The simulations elucidate the behavior of high-rate, lithium-ion batteries under abuse testing based on the best available knowledge of the reactions that take place. The simulations identify the determining factors in thermal runaway. Further experimental work could verify these factors. Specifically, experimental studies to determine how effectively the electrolyte competes with the binder could help elucidate the role of the binder. Biensan et al. [4] have reported DSC results showing the heat evolved from a charged negative electrode is proportional to the amount of PVDF binder, while Maleki et al. [10] report the heat evolved increases with state of charge of the negative. However, in both cases, the electrodes were dried to eliminate competing solvent reactions. Repeating these studies with wet electrodes (electrodes saturated in electrolyte) to see if the total heat evolution still increased with the amount of binder would reveal if the reactions involving PVDF binder can successfully compete with those involving electrolyte.

With experimental data, the parameters in the simulations shown here can be adjusted to fit that data. The parameters used were based on a review of published literature, and oftentimes, there was some ambiguity in how to interpret the parameters. Access to raw experimental data would remove that ambiguity. In addition, the simulations carried out here are based on a very approximate depiction of the real physical system. For example, there is uncertainty in the role of the salt. The salt has been implicated in solvent decomposition, negative/solvent reactions, and the positive/solvent reactions, but its role is unclear. The mechanisms of all the reactions are not well characterized, and probably involve several steps, so the overall reaction rates may not follow simple Arrhenius laws. However, given the present understanding of lithium-ion chemistry, the approach used here is a reasonable means to guide further work.

Acknowledgements

R.S. expresses appreciation for NSF Award DMI-0109141 for partial support of this work.

References

[1] R. Venkatachalapathy, C.W. Lee, W. Lu, J. Prakash, Electrochem. Commun. 2 (2000) 104–107.
[2] Z. Zhang, D. Fouchard, J.R. Rea, J. Power Sources 70 (1998) 16–20.
[3] H. Maleki, G. Deng, A. Anani, J. Howard, J. Electrochem. Soc. 146 (9) (1999) 3224.
[4] Ph. Biensan, B. Simon, J.P. Peres, A. de Guibert, M. Broussely, J.M. Bodet, F. Perton, J. Power Sources 81–82 (1999) 906–912.
[5] K.-K. Lee, W.-S. Yoon, K.-B. Kim, K.-Y. Lee, S.-T. Hong, J. Electrochem. Soc. 148 (7) (2001) A716.
[6] W. Lu, C.W. Lee, R. Venkatachalapathy, J. Prakash, J. Appl. Electrochem. 30 (2000) 1119.
[7] M.N. Richard, J.R. Dahn, J. Electrochem. Soc. 146 (1999) 2068.
[8] D.D. MacNeil, J.R. Dahn, J. Phys. Chem. A 105 (2001) 4430–4439.
[9] G.G. Botte, R.E. White, Z. Zhang, J. Power Sources 97–98 (2001) 570–575.
[10] H. Maleki, G. Deng, I. Kerzhner-Haller, A. Anani, J.N. Howard, J. Electrochem. Soc. 147 (12) (2000) 4470.
[11] C. Lampe-Onnerud, J. Shi, R. Chamberlain, P. Onnerud, in: Proceedings of the 16th Annual Battery Conference on Applications and Advances, IEEE, Long Beach, CA, 2001.
[12] T.D. Hatchard, D.D. MacNeil, A. Basu, J.R. Dahn, J. Electrochem. Soc. 148 (7) (2001) A755–A761.
[13] H. Arai, M. Tsuda, M. Hayashi, Y. Sakurai, ECS Meeting, Phoenix, October 2000.
[14] D. Fouchard, L. Xie, W. Ebner, S.A. Megahed, Rechargeable lithium and lithium ion (RCT) batteries, in: S.A. Megahed (Ed.), Electrochemical Society PV 94-28, Miami Beach, Florida, October 1994.
[15] U. von Sacken, E. Nodwell, A. Sundher, Solid State Ionics 69 (1994) 284–290.
[16] D.D. MacNeil, T.D. Hatchard, J.R. Dahn, J. Electrochem. Soc. 148 (7) (2001) A663.
[17] C. Menahem, D. Golodnitsky, E. Peled, Batteries for portable applications and electric vehicles, in: C.F. Holmes, A.R. Landgrebe (Eds.), Electrochemical Society PV 97-18, Paris, France, September 1997.
[18] A. Du Pasquier, F. Disma, T. Bowmer, A.S. Gozdz, G. Amatucci, J.-M. Tarascon, J. Electrochem. Soc. 145 (2) (1998) 472–477.

[19] K. Kanari, Y. Saitoh, T. Masuda, in: Proceedings of the 15th Japan Symposium on Thermophysical Properties, 1994, pp. 465–468.
[20] H. Maleki, S.A. Hallaj, J.R. Selman, R.B. Dinwiddle, H. Wang, J. Electrochem. Soc. 146 (3) (1999) 947–954.
[21] T. Horiba, K. Hironaka, T. Matsumura, T. Kai, M. Koseki, Y. Muranaka, in: Proceedings of the First Annual Advanced Automotive Battery Conference, Las Vegas, NV, 2001.
[22] G. Chagnon, P. Allen, K. Hensley, K. Nechev, S. Oweis, R. Reynolds, A. Romero, T. Sack, M. Saft, in: Proceedings of the First Annual Advanced Automotive Battery Conference, Las Vegas, NV, 2001.
[23] K. Kitoh, H. Nemoto, J. Power Sources 81–82 (1999) 887–890.
[24] S. Tobishima, J. Yamaki, J. Power Sources 81–82 (1999) 882–886.
[25] Y. Saito, K. Takano, A. Negishi, J. Power Sources 97–98 (2001) 693–696.
[26] R.A. Leising, M.J. Palazzo, E.S. Takeuchi, K.J. Takeuchi, J. Electrochem. Soc. 148 (8) (2001) A838–A844.
[27] H. Maleki, G. Deng, J. Howard, in: Proceedings of the Electrochemical Society Meeting, San Francisco, 2001.
[28] E.P. Roth, G. Nagasubramanian, D.R. Tallant, M. Garcia, SANDIA Report SAND99-1164, 1999.
[29] D.D. MacNeil, D. Larcher, J.R. Dahn, J. Electrochem. Soc. 146 (10) (1999) 3596.
[30] S.E. Sloop, J.K. Pugh, S. Wang, J.B. Kerr, K. Kinoshita, Electrochem. Solid-State Lett. 4 (4) (2001) A42.
[31] J.-S. Kim, J. Prakash, J.R. Selman, Electrochem. Solid-State Lett. 4 (9) (2001) A141.
[32] D.D. MacNeil, D. Larcher, J.R. Dahn, J. Electrochem. Soc. 148 (11) (2001) A1211.
[33] S. Al Hallaj, H. Maleki, J.S. Hong, J.R. Selman, J. Power Sources 83 (1999) 1–8.
[34] J.R. Dahn, Lithium-Ion Battery Tutorial and Update: Power 2001, Anaheim, CA, September 30 2001.
[35] Y. Chen, J.W. Evans, J. Electrochem. Soc. 143 (9) (1996) 2708–2712.
[36] K. Kanari, K. Takano, Y. Saito, T. Masuda, in: Proceedings of the International Workshop on Advanced Batteries, Osaka, 1995.
[37] N. Sato, J. Power Sources 99 (2001) 70–77.
[38] A. Funahashi, Y. Kida, K. Yanagida, T. Nohma, I. Yonezu, J. Power Sources 104 (2002) 248–252.
[39] T.F. Fuller, M. Doyle, J. Newman, J. Electrochem. Soc. 141 (4) (1994) 962–990.
[40] S.V. Patankar, Numerical Heat Transfer and Fluid Flow, Taylor & Francis, London, 1980.
[41] A.C. Hindmarsh, A.G. Taylor, User Documentation for IDA: A Differential-Algebraic Equation Solver for Sequential and Parallel Computers, Lawrence Livermore National Laboratory, UCRL-MA-136910, 1999.
[42] K. Kanari, Y. Saitoh, T. Masuda, in: Proceedings of the 15th Japan Symposium on Thermophysical Properties, 1994.
[43] T. Kawamura, A. Kimura, M. Egashira, S. Okada, J.-I. Yamaki, J. Power Sources 104 (2002) 260–264.
[44] H. Arai, M. Tsuda, K. Saito, M. Hayashi, Y. Sakurai, J. Electrochem. Soc. 149 (4) (2002) A401–A406.